Diffraction analysis of a disordered surface, modelled on a probability distribution of reconstructed blocks: $Bi/Si(001)-(2\times n)$, n = 6.45

1999 J. Phys.: Condens. Matter 11 1935

(http://iopscience.iop.org/0953-8984/11/8/007)

J. Phys.: Condens. Matter **11** (1999) 1935–1951. Printed in the UK PII: S0953-8984(99)98095-5

Diffraction analysis of a disordered surface, modelled on a probability distribution of reconstructed blocks: Bi/Si(001)-(2 × n), n = 6.45

N Jedrecy†‖, L Gavioli‡, C Mariani‡, M G Betti‡, B Croset§ and C de Beauvais§

† LURE, CNRS-MRES-CEA, Bâtiment 209 D, Centre Universitaire Paris Sud, BP 34, F-91898 Orsay Cédex, France, and Laboratoire de Minéralogie-Cristallographie, Associé au CNRS et aux Universités Paris 6 et Paris 7, 4 Place Jussieu, F-75252 Paris Cédex 05, France

‡ Dipartimento di Fisica, Università di Modena, via G Campi 213/A, I-41100 Modena, Italy

§ Groupe de Physique des Solides, UMR CNRS 75-88, 2 Place Jussieu, F-75251 Paris Cédex 05, France

Received 5 October 1998

Abstract. Bismuth adsorbs on the Si(001)-(1 × 2) surface in the form of rows of dimers. Missing-dimer lines (MDLs) are created perpendicularly every n units, leading to (2 × n) periodicity. Depending on the coverage, n can vary from 12 to 5. We investigated by grazing incidence x-ray diffraction the (2 × n) structure, with $n = 6.45$. The disorder in the MDL periodicity, as well as the defects along the MDL, reduce considerably the correlation length of the reconstructed domains. As a consequence, the integrated intensity of each reflection must be corrected, evaluating the trace of the resolution function across the diffraction node. The structural refinement, based on the as-derived intensities, provides the Bi dimer bond length (3.11 Å), the Si atom positions (bulklike), and the height of the Bi plane with respect to Si (1.88 Å). In addition, we give evidence that the dimers are displaced along the row from ideal positions towards the MDL (from 0.15 to 0.50 Å). Last, the diffraction profiles are calculated, on the basis of a probability distribution of (2 × n) cells (n = 6, 7, 1), using the phase-matrix method. The average positions of the fractional peaks are related to the concentration of each type of cell. The width and the intensity of the second order peaks, compared to those of the first order peaks, allow us to account for the aggregation tendency.

1. Introduction

Group V semimetal adsorption on clean semiconductor surfaces gives rise to non-reactive and non-interdiffusing interfaces, which are model systems to understand the relationship between the atomic structure and the electronic properties. Annealing of an As overlayer on Si(001)-(2 × 1) is known to produce an ordered monolayer, with (2 × 1) symmetry attributed to metal dimer formation. In the case of Sb, small (2 × 1) domains are formed, separated by large bare areas. One can observe with Bi a series of (2 × n) symmetry phases, with n varying continuously and irreversibly from $n = 12$ to $n = 5$ as a function of the thermal treatment [1, 2]. If the phenomenon of uniaxial phase transitions is commonly observed on metal surfaces [3, 4], only a few examples are known on semiconductor surfaces. Moreover, bismuth is a candidate for the passivation of the chemically reactive Si(001) surface. Recently,

‖ Author to whom correspondence should be addressed. Fax number: 33 1 64 46 41 48. E-mail address: jedrecy@lure.u-psud.fr.

0953-8984/99/081935+17$19.50

it was found as a surfactant as well in the heteroepitaxial growth of Ge on Si [5]. The present study deals with the $(2 \times n)$ Bi/Si interface, with n between 6 and 7.

When deposited on Si(001) at room temperature, bismuth forms three-dimensional (3D) islands after the completion of the first monolayer (ML). The 3D islands start to desorb at 200 °C, leaving a two-dimensional (2D) ordered Bi overlayer, when the coverage reaches the monolayer regime. Considering the 1 ML (2×1)-Bi/Si(001) interface, with rows of Bi dimers, the $(2 \times n)$ structure is obtained by removing every nth Bi dimer, and ordering such missing-dimer defects in lines perpendicular to the dimer rows (figure 1). One should notice that the $(2 \times n)$ ordering is also observed with a controlled adsorption of Bi above 0.5 ML [6].

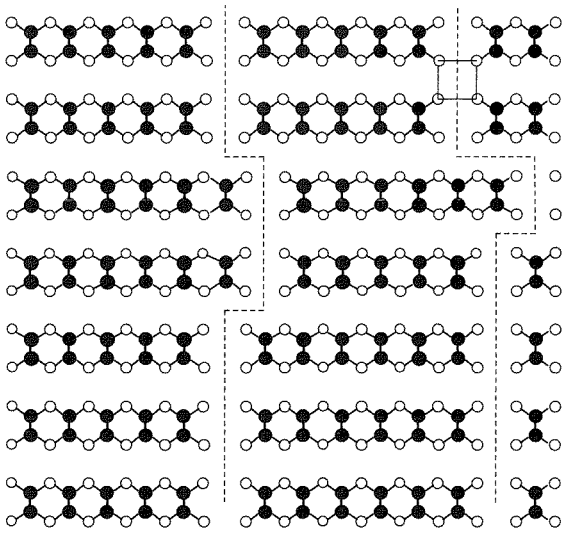

Figure 1. Projected view of the Bi/Si(001)-$(2 \times n)$ surface, the topmost Bi layer ordering in (2×6) and (2×7) unit cells, on top of a Si layer in its bulk (1×1) configuration. The dashed line is a guide for the missing-dimer line. Kinks occur when a (2×7) cell succeeds a (2×6) cell in the $(\times 2)$ direction.

The missing-dimer defect model has been first proposed in the case of the clean Si(001)-$(2 \times n)$ surfaces (n ranging between 6.5 and 9.6) obtained by quenching from high temperatures [7, 8]. A recent paper reports the formation of the $(2 \times n)$ missing-dimer line network on Bi/Ge(001) [9]. Considering that group V elements adsorb on Si or Ge(001) surfaces in the form of aligned dimers, taking into account the atomic sizes of Sb or Bi with respect to Si or Ge, one expects that a compressive stress develops along the dimer row. The missing-dimer defect enables such compressive strain energy to be relieved. As a matter of fact, a high density of voids or antiphase defects is observed on the (2×1)-Sb/Si surface [10]. The specificity of Bi is that the vacancies order into lines, with an nth order periodicity. This can be explained by considering long-range repulsive interaction between the defect lines, and short-range attractive interaction between vacancies in adjacent rows [11]. The assumption of an electrostatic field between the vacancy lines may be correlated to what happens with the graphite intercalation compounds (GICs), whose phase diagrams could be predicted [12, 13].

Scanning tunnelling microscopy (STM) images on the Bi/Si(2×7) surface attest to the long-range ordering of missing rows, despite the presence of some defects, like 3D Bi clusters, rectangular or linear vacancies, and kinks along the missing-dimer lines [2]. A shift in the dimer direction of some parts of the dimer rows is also a possible defect, reported as a dislocation-

type defect [14]. The STM images support the idea that the continuous change of n does not result from a continuous change of the dimer spacing, but rather from a fluctuating periodicity of the missing rows on the surface (see figure 1). When n is equal to 5, large voids alternate with small (2×5) dimer blocks. When n approaches 10, the MDL spacing becomes poorly periodic because of the kinks [2].

The grazing incidence x-ray diffraction (GIXD) technique, used in the present work, allows the structural determination of the $(2 \times n)$-Bi/Si(001) surface, with $n = 6.45$. The surface, a mixture of (2×6) and (2×7) unit cells, is quantitatively analysed in terms of an $n = 6$ or $n = 7$ surface. The refinement procedure confirms the missing-dimer model and provides the atomic positions of the Bi and Si first layer atoms. In particular, evidence is given for the lateral expansion of the Bi layer with respect to Si. The $n = 6.45$ periodicity is analysed using the phase-matrix-method formalism [15]. The $(2 \times n)$ ($n = 6, 7$) cell concentration, as well as the probability value for the $(2 \times n)$ cell to be followed by the same type of cell, are derived.

2. Experimental details

The Si(001) substrates ($13 \times 13 \times 2.5$ mm^3), prior cleaned using the Shiraki chemical etch, were outgassed at 500 °C into the ultra-high-vacuum (UHV) growth chamber for several hours, before several flash-annealings up to 1000 °C. The procedure is known to produce high-quality two-domain (2×1)-(1×2) surfaces [16]. Bismuth was deposited at room temperature from a Knudsen cell at 480 °C, up to 4 ML. The coverage calibration has been based on the Auger peak-to-peak intensity ratio. The samples were then annealed at increasing temperatures, following the Bi desorption by high-energy or low-energy electron diffraction (RHEED or LEED). On the 4 ML thick film, RHEED shows rings associated with the 3D Bi islands, while a 2D pattern is obtained above 200 °C. Diffuse extra spots, at $\pm 1/n$ from the integer order reflections, with n between 6 and 7, could be identified by LEED, after annealing at 350 °C. A special procedure was followed to ensure cleanliness of the Si surface before deposition. The sample was then quickly transferred in the coupled six-circle diffractometer. Indeed, our chamber being used for GaAs growth, As residuals, even at a very low concentration, are present. We noticed that Bi adsorption was very sensitive to them, while the long-range ordering of the Si dimers on the clean Si(001) surface is not affected [16].

The apparatus is installed on the wiggler beam line DW12 of the DCI storage ring at LURE (Orsay). We used a focused radiation at a wavelength of 0.887 Å. The Bi/Si sample surface was set to the critical angle for total external reflection during all data collection. In addition, comparative measurements were performed, using same conditions, on a clean Si surface, issued from the same set of wafers.

As shown by STM, the $(2 \times n)$ arrangement does not repeat itself more than about n times. The long-range order, as mentioned up to now, is in fact quite weak for x-ray diffraction. The width of the fractional peaks acts as the inverse of the coherent domain size. The latter provided a node size in the reciprocal space, larger than the resolution function provided by the angular acceptance of the x-ray detector. The intensity is not fully integrated when scanning across a node. Specific corrections were established for the normalization of the data.

Among the 33 reflections of the final set, 16 were estimated with large standard deviations. Six profiles were overlapped with large parasitic peaks, and ten had very weak intensities. In the latter case, the parasitic contributions had amourphous-like structure, and could be associated with the 3D Bi clusters on top of the ordered layer. In particular, two azimuthal orientations could be determined, the a axis of the bulk Bi hexagonal structure being parallel to the $\langle 110 \rangle$ Si direction.

3. Analysis of the superlattice nodes

During the time of data collecting (4 days), no changes on the reference reflections were observed, attesting that the clean Si(001) surface is highly passivated by Bi atoms. The two 90° rotated domains, $(2 \times n)$ and $(n \times 2)$, were found to be equally probable. The half-order reflections were revealed to be of the same order of magnitude as the nth order ones, in contrast to what is reported for RHEED intensities [1]. Besides, referring to a momentum transfer $\boldsymbol{q} = h\boldsymbol{a}^* + k\boldsymbol{b}^* + l\boldsymbol{c}^*$, where $\boldsymbol{a}^*$, $\boldsymbol{b}^*$, $\boldsymbol{c}^*$ are the reciprocal space (RS) vectors of the conventional 1×1 unit cell, it turned out that the $(p - 1/n, k, 0.04)$ reflections (p integer) were stronger than the $(p + 1/n, k, 0.04)$ ones. No signal was registered at $(p \pm i/n, k, 0.04)$, when $i > 1$, in agreement with LEED observations. This point is explained by the fact that the interface structure is mainly (1×2), with a modulation every n units along the dimer chain. The first point suggests that the spacing between Bi dimers is slightly elongated with respect to the ideal position of the Si atoms.

The x-ray superlattice nodes were unexpectedly spread out in reciprocal space. Usually, fractional and integer order node widths are of the same order of magnitude. They are equal if each reconstructed domain extends over a whole terrace. If anti-phase boundaries exist between domains on top of a terrace, the fractional reflection widths are larger, up to five times the width of the integer orders. On the clean Si surface, the two types of node have the same width, around 0.5×10^{-3} Å^{-1}. On the (2×6.45)-Bi/Si interface, the fractional node widths are 23.8×10^{-3} Å^{-1} in the $(\times 2)$ direction and 35.8×10^{-3} Å^{-1} in the $(\times n)$ direction, while integer order nodes have the same width, 1.22×10^{-3} Å^{-1}, in both directions. Plots of representative reflection profiles ((1.5, 0, 0.04) and (1, 0, 0.04)) are shown in figure 2. One can deduce for the Bi/Si interface a coherent domain size of 800 Å for the Si terraces. Using the same approach to estimate the coherent size of the $(2 \times n)$ domains would lead to an average value of 35 Å. This value is in agreement with the STM images, which show that the ideal (2×7) cell does not repeat itself more than about seven times. Indeed, defects occur, such as the missing-dimer cluster or the kink in the missing-dimer line. These defects are expected to break the coherence in the diffracting process. In the case of an average $(2 \times n)$ periodicity, the node extension is also related to the probability of finding a missing dimer along a dimer row after six or seven Si units. Fortunately, the knowledge of the missing-dimer line distribution is not necessary to analyse the integrated intensities, as will be exposed in section 6.

An important effect of the large node widths is that part of the integrated intensity is not measured. In the case of in-plane reflections, the intensity is usually integrated over one in-plane direction (in-plane detector aperture), while the scanning provides the intensity in the in-plane perpendicular direction [17]. In the case of out-of-plane reflections, the intensity may be obtained in the same way, by performing the scans parallel to the surface plane (z-axis mode). However, one has to take into account the out-of-plane detector aperture, with respect to the height of rod intersecting the Ewald sphere. A typical scan is the rotation of the sample around its surface normal (ϕ-scan). When the resolution function is perpendicular to the scanning direction, the width of the peak gives the size of the node along that direction. The node sizes along the $(\times 2)$ and $(\times n)$ directions are estimated by use of reflections with such geometry (for instance, (1.5, 0, 0.04) is well suited to evaluate the node size along the $(\times n)$ axis). The size of the resolution function is given by $\Delta q_r = \Delta s/(\lambda D)$, where Δs is the in-plane aperture of the slits in front of the detector, λ is the wavelength and D is the distance between the sample and the detector. In the present case, the nodes are too wide for the intensity to be integrated along one direction at fixed position. Figure 3 presents the reflection (1.5, 1, 0.04) from the $(2 \times n)$ domains within the experimental geometry. Three types of scan are sketched, the ϕ-scan, the h-scan, and the k-scan. The crossing of the node through the Ewald sphere is understood as a

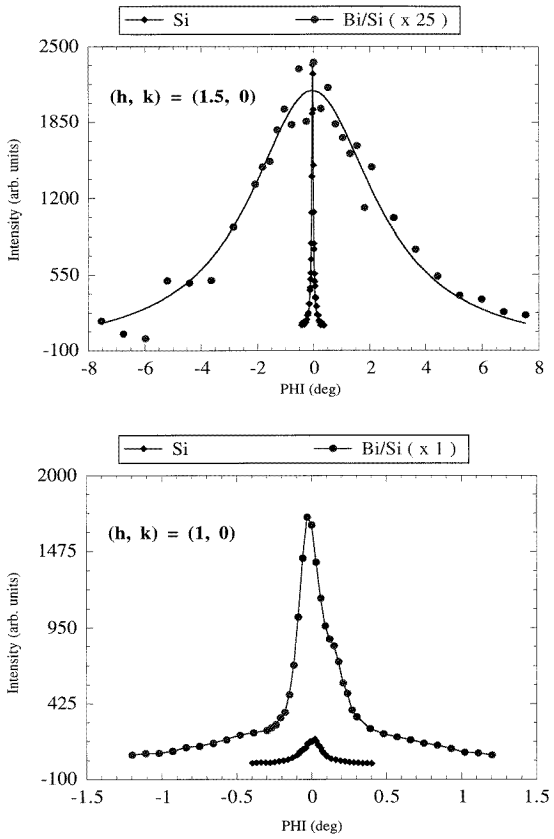

Figure 2. Rocking curves of integer and fractional reflections from the Si(001)-(2 × 1) and the Bi/Si(001)-(2 × n) surfaces.

scan of the resolution function through the node, along the dashed lines. The node associated to the clean Si surface is shown for comparison.

After the usual corrections specific to the z-axis geometry, the data set was normalized, taking into account the areas crossed by the resolution function. In most common cases, the scan profiles are Lorentzian-like. We write $\Lambda(h, k)$, the two-dimensional (2D) intensity distribution of the nodes, where h, k, are the deviations from the centre of the node. Vlieg [17] has derived the $\Lambda(h, k)$ form in the case of an isotropic node, so as to ensure that, if the node is fully integrated along one direction (for instance k), the profile along the perpendicular direction is a true Lorentzian. We consider the node projected in the plane of the surface as an ellipsoide, and write the distribution function as

$$\Lambda(h,k) = \frac{1}{2uv\pi}\frac{1}{[1+(h/u)^2+(k/v)^2]^{3/2}}$$

where u and v are the half width at half maximum (HWHM).

One can verify that integrating this function along k from $-\infty$ to $+\infty$ leads to a 1D Lorentzian line shape along h. The experimental intensity has to be corrected, evaluating the portion C of the node crossed by the resolution function.

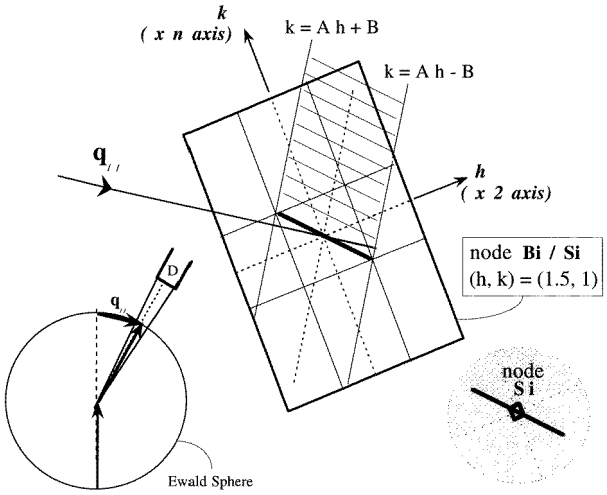

Figure 3. A schematic drawing of the resolution function (thick line) with respect to the intensity distribution of the in-plane node (1.5, 1), assumed as rectangular. Three possible scans are shown as dashed lines, with emphasis on the rocking scan. The resolution function is provided by the acceptance of the detector; the Ewald construction is shown as an inset.

In the case of a rocking scan (ϕ-scan),

$$C = \int_{-\infty}^{+\infty} \mathrm{d}h \int_{Ah-B}^{Ah+B} \Lambda(h,k)\,\mathrm{d}k$$

where ($k = Ah - B$) and ($k = Ah + B$) are the straight lines delimiting the trace of the resolution function (see figure 3). Defining ϕ as the angle between the in-plane $\boldsymbol{q}_\parallel$ vector ($q_\parallel = h\boldsymbol{a}^* + k\boldsymbol{b}^*$) and the $\boldsymbol{a}^*$ axis, and β as the angle between the resolution function and $\boldsymbol{q}_\parallel$, A and B are given by:

$$A = 1/|\tan\phi|$$

$$(2B) = \Delta q_r \cos\beta/|\sin\phi|.$$

For in-plane reflections, β is the Bragg angle. The cases $\phi = 0^\circ$ and $\phi = 90^\circ$ correspond to a k-scan and an h-scan, respectively.

In the case of an h-scan,

$$C = \int_{-\infty}^{+\infty} \mathrm{d}h \int_{-B'}^{+B'} \Lambda(h,k)\,\mathrm{d}k$$

where $(2B') = \Delta q_r|\sin(\beta + |\phi|)|$.

In the case of a k-scan,

$$C = \int_{-\infty}^{+\infty} \mathrm{d}k \int_{-B''}^{+B''} \Lambda(h,k)\,\mathrm{d}h$$

where $(2B'') = \Delta q_r|\cos(\beta + |\phi|)|$.

When B is large with respect to u or v, one retrieves, after integration along h, the 1D Lorentzian profile. We derived the correction factors numerically. If one wants to obtain analytical results for C, one should use other forms for $\Lambda(h,k)$ than the ellipsoidal distribution. A possible choice is the simple product of two 1D Lorentzians with respective HWHM u and v.

We investigated different quadrants of the reciprocal space, considering the $(2 \times n)$ as well as the $(n \times 2)$ domains. The validity of the corrections was assessed by the close intensity values obtained from different types of scan, performed on the same reflection. More than 100 in-plane reflections were measured, as well as six rods up to an out-of-plane momentum transfer $qz = 3.24$ Å^{-1}. After reduction by the $2mm$ symmetry, a coherent set of 33 independent in-plane reflections and five rods was obtained. The structural refinement was guided by the usual χ^2-factor, although the R-factor was considered too [18].

4. The 2×6 and 2×7 models

The fitting procedure was first undertaken using a (2×6) cell, modifying the indices of the superlattice reflections according to this choice. The calculation has taken into account the contribution from the (6×2) domains in the case of the integer order nodes. The (2×6) surface cell vectors are, with respect to the conventional FCC Si lattice: $\boldsymbol{a}^s = 2/2\,[110]$, $\boldsymbol{b}^s = 6/2\,[\bar{1}10]$ and $\boldsymbol{c}^s = [001]$.

A reduced set (I) of 17 in-plane structure factors was considered, as a starting point, the 16 reflections with larger error bars (see section 2) constituting the set (II). The reflections with the k index multiple of 6 are mainly sensitive to the Bi dimer bond length, and can even be treated within the framework of a (2×6) cell with six dimers aligned, as if the surface were (2×1). The sixth order reflections necessitate, in the dimer vacancy model, outwards displacements of the dimers along the row. Considering the model sketched in figure 4, we assumed a single bond length for all dimers, and the same displacement along the dimer direction (x) for the Si atoms. As a first choice, the fitting parameters were the dimer bond length, the displacement of dimer 3 along the row (y) forced to be twice the value of the dimer 2 displacement, the Si atom displacement along x and the Debye–Waller factor B of Bi atoms. The factor B is related to the root-mean-square thermal displacement $\sqrt{u^2}$, by $B = 8\pi^2 u^2$. It was set at the bulk value, 0.45 Å^2, for the Si atoms. We obtain a χ^2 residual of 1.4, corresponding to a Bi dimer bond length of 3.130 ± 0.003 Å, outward displacements of dimers 2 and 3 by 0.26 and 0.52 Å from their ideal positions, respectively, and a B factor of 2.2 ± 0.2 Å^2, leading to a thermal amplitude of 0.17 Å. Finally, the first layer Si atoms remain basically in their bulk positions (± 0.08 Å).

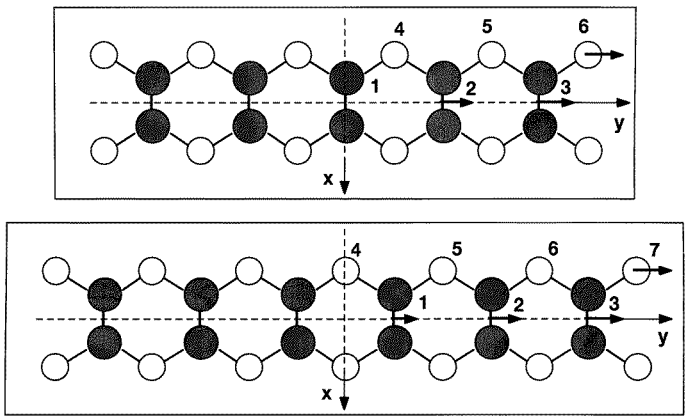

Figure 4. Projected structural models ((2×6) and (2×7) unit cells), with indication of atoms allowed to move in the refinement. The arrows represent the main atomic displacements. The symmetry planes are shown as dashed lines.

Introducing the data set II, the Bi dimers 2 and 3 are allowed to move along y independently, while the bismuth B factor is fixed at 2.2 Å^2. We obtain a fit with $\chi^2 = 1.16$, corresponding to a dimer bond length d of 3.11 Å, Si atoms displaced outwards along x by 0.14 Å and Bi dimers 2 and 3 moved outwards along y by 0.26 and 0.45 Å, respectively. By setting the Si atoms at bulk positions, the χ^2 is not significantly changed (1.26), as well as the other parameter values ($d = 3.12$ Å and Bi dimers are displaced by 0.28 and 0.47 Å).

It is possible to improve the χ^2-value by adding more parameters in the fit. For instance, $\chi^2 = 1$ is obtained using a similar model where the Si atoms 4, 5, 6, are moved along the row direction (y) by -0.3, 0.6 and 0.2 Å, respectively. This leads to the observation that large Si atom displacements along y introduce only small changes in the χ^2-value. Indeed, the Si contribution to the integrated intensities is weak compared to that of Bi, due to the different scattering factors. On the other hand, an inwards Si displacement along x by 0.15 Å induces a significant increase (a factor of two) in the χ^2-value. Thus, the current data set does not allow us to confidently determine the Si atom positions along y. However, one can retain a model, with Si atoms 4 and 5 fixed at their y bulk positions, leaving the y position of Si number 6 free. This model gives a χ^2 of 1.1, with the Si atom 6 displaced along y by 0.7 Å. Such position is compatible with a dimerization along the Bi dimer row of the Si atoms near the vacancy. The Si dimer bond length is 2.44 Å, close to the value found in the case of the clean Si surface. The final R-factor is equal to 5.6%.

To summarize, the best structural parameters, corresponding to the observed and calculated structure factors listed in table 1, are the following:

- Bi dimer bond length $d = 3.12 \pm 0.01$ Å,
- Bi dimers 2 and 3 displaced outwards along the row (y-direction) by 0.28 and 0.50 Å (± 0.02 Å), respectively;
- Si atoms in the first layer displaced in the x-direction by 0.05 ± 0.05 Å,
- dimerized Si atoms near the vacancy,
- a Debye–Waller factor for bismuth $B = 2.2 \pm 0.2$ Å^2.

Table 1. Comparison between observed and calculated in-plane structure factors, using the (2×6) surface model.

Set (I)					Set (II)				
h	k	F_{calc}	F_{obs}	s_{obs}	h	k	F_{calc}	F_{obs}	s_{obs}
3	0	120.9	113	30	1	12	14.1	31	30
1	6	41.2	37	10	3	12	32.5	20	20
3	6	91.7	105	30	4	5	31.7	34	30
5	6	88.8	88	20	4	7	8	0	10
1	0	71.3	79	20	4	17	35	59	50
2	0	187.2	144	20	4	19	7.7	0	10
4	6	19.6	25	5	2	7	26.2	45	20
6	0	24.3	22	10	4	13	19.9	55	40
6	6	20.6	49	10	6	13	2.6	0	10
8	6	47.9	46	10	6	11	21	0	10
10	6	33.1	28	5	2	13	40.1	45	20
2	6	99.1	100	40	6	5	9	32	30
0	17	105	109	30	6	13	2.6	7	7
0	5	112.8	118	20	6	12	17.7	22	5
2	17	83.1	92	30	6	18	9	9	5
2	5	84.7	74	20	8	18	2.6	10	5
2	11	94.7	128	20					

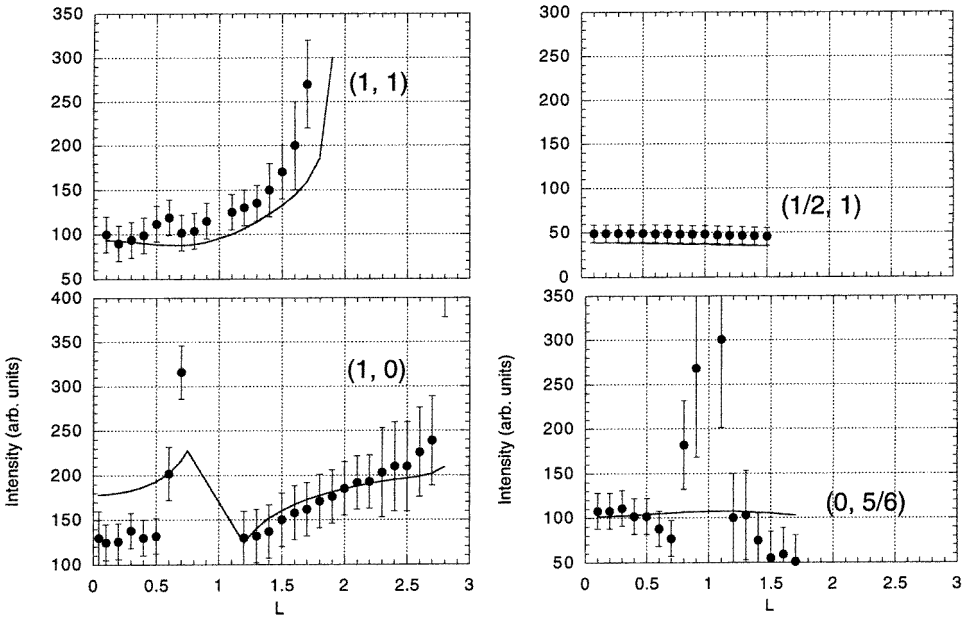

Figure 5. Comparison between measured and fitted rods.

With this model, the rods have been incorporated into the data set II, adding as fitting parameters the out-of-plane positions of the Bi dimers and the Si first layer atoms. Two superlattice rods, (0, 5/6) and (1, 11/6), cannot be considered over the whole scanned l range. For instance, for rod (0, 5/6), shown in figure 5, there is a contribution near $l = 1$, from the bulk allowed Si reflection at $l = 1$ on the neighbouring integer rod (0, 1). Indeed, the lateral extension of the fractional rods implies large scans, and the detector catches intensity from bulk Si reflections, which cannot be estimated in the kinematical theory approach. The main information provided by the superlattice rods is their profile flatness, in agreement with our conclusions on one-level (001) Bi and Si first planes, without displacements in the deepest layers. Actually, tests of the asymmetric model for Bi dimers have been performed, but Bi atoms have been systematically brought back to the same z-height. This occurs also considering separately asymmetric Bi dimers.

An overall χ^2 of 2.33 is obtained with the in-plane parameters determined previously, a Bi layer at 1.86 ± 0.05 Å from the first Si layer and the Si plane displaced outwards by 0.3 ± 0.1 Å from the bulk position. These values result in a Bi–Si bond length of 2.68 Å. The strong displacement obtained for the first Si layer could be due to the fact that only this layer is allowed to relax, while the displacements in the deepest layers should be considered as well. Actually, the χ^2 can be reduced (1.65) by letting the heights of the second and third Si planes be free, as well as the x-positions of the fourth and fifth layers (taking into account the tetrahedral symmetry of the Si orbitals). However, this results mainly from the large error bars on the structure factors. Looking at the calculated rods, one observes modulations in the intensity profiles, that clearly do not emerge in the experimental rods. We conclude that the pertinent parameter is the Bi dimer height with respect to the first Si plane; as a confirmation, it is found at 1.9 Å leaving the Si plane at the bulk position.

A (2×7) unit cell model (see figure 4) was also considered. The fitting procedure is similar to the one used for the (2×6) structure. A χ^2 of 1.0 is obtained with the in-plane data set, while incorporating the rods leads to an overall χ^2 of 2.0. The structural parameters are the following:

- a Bi dimer bond length $d = 3.10 \pm 0.02$ Å,
- Bi dimers 1, 2 and 3, displaced outwards along the row (y-direction) by 0.15 ± 0.05 Å, 0.3 ± 0.05 Å and 0.45 ± 0.02 Å, respectively,
- Si atoms in the first layer at -0.015 ± 0.015 Å from the x bulk position,
- a Debye–Waller factor for bismuth $B = 2.2 \pm 0.2$ Å^2,
- a Bi plane lying at 1.9 ± 0.01 Å from the first Si plane, fixed at the bulk position.

5. Discussion

The deviations associated with the structure factors preclude us from estimating all the atomic positions with accurate precision. Nevertheless, the experiment allows several assertions. The value obtained for the Bi dimer bond (3.12 or 3.10 Å, depending on the unit cell assumption), is close to the value that can be deduced from the atomic radius of Bi (3.1 Å). This suggests that the Bi atoms preserve their group V electronic configuration after adsorption on Si. Nevertheless, the underlying Si atoms are found at or close to the bulk positions, thus attesting that the Si dimers of the clean surface have been broken, a (1×2)-Si domain being changed into a ($2 \times n$)-Bi/Si domain. The bonds formed between Bi and Si promise a compressive strain along the Bi dimer row will develop, due to the mismatch between atomic radius of Si (1.2 Å) and Bi (1.55 Å). As a matter of fact, in addition to the vacancy defect formation, the Bi dimers are displaced laterally, up to 0.5 Å along the row, with respect to Si. This particular configuration of the Bi dimers is not considered in any of the theoretical models, which assimilate the Bi surface to a (2×1) one [19, 20].

The calculations, based on total energy and atomic forces, led to the following results. Assuming an ideal bulk terminated Si surface, the first models gave a Bi dimer bond length of 3.14 Å [19]. Despite a reduction of the binding energy for a Bi dimer adsorbed on Si(001)-(1×2) compared to Si(001)-(1×1), the second structure has been found to be lowered in energy, when considering a Bi coverage above 0.5 ML. More recent calculations suggest that without Si relaxation the dimer bond length is 3.21 Å, while it changes to 3.16 Å when including Si relaxation. Moreover, the height of the Bi plane relative to an ideal Si plane is found at 1.88 Å and 1.8 Å, respectively. In the latter case, a 0.05 Å inward relaxation of the first Si layer is obtained, leading to a Bi dimer at 1.85 Å on top of the Si(001) plane and an Si–Bi bond length of 2.68 Å. The (2×1) simplifying assumption is also used in an x-ray standing wave (XSW) analysis [20]. A Bi bond length of 2.94 ± 0.06 Å is reported, with a dimer height of 1.73 Å on top of the ideal Si surface, and a B-factor of 1.8. The bond length values differ from each other depending on the mode of calculation. For instance, a small relaxation of the Si layer affects strongly the dimer bond length value. Considering the strain relaxation inside the Bi overlayer, provided by the displacements of the dimers towards the vacancy defect, new total-energy calculations are expected. Last, we underline the fact that the large error bars along the rods precluded us from considering displacements in the second and third layers, thus leading to unreliable determination of the first Si plane height. However, the relative heights of the Bi and Si(001) planes are found to be the same as the predicted values.

6. Analytical treatment of the diffracted intensity

6.1. Model for the disorder between the blocks of dimers

We manage to reproduce the integrated intensities by use of a $(2\times n)$ cell with $(n-1)$ Bi dimers and one missing dimer (MD), taking either $n = 6$ or $n = 7$. The two models differ only by the number of dimers inside a block, the atomic positions leading to an average spacing close to 4.1 Å. The experimental periodicity $n = 6.45$, derived from the position of the peaks at $\pm p/n$ from the integer orders ($p = 1, 2$), issues from the disorder between the (2×6) and (2×7) cells. We will demonstrate in the following that the refinement process is valid disregarding the disorder between the cells, if using the first order satellites alone ($p = 1$). We calculate analytically the intensity scattered by a probability distribution of (2×6) and (2×7) cells. We demonstrate that the average periodicity is, at first order, related to the concentration of each type of cell. The shape and the intensity of the second order peaks ($p = 2$), compared to those of first order, are related to the aggregation tendency of each type of cell. In order to reproduce the widths of the peaks, we use a small value $\overline{N}$ for the average number of cells diffracting coherently along the $(\times n)$ axis. To obtain reasonable $\overline{N}$ values, one has to introduce a third object. This third object is for instance a (2×1) cell without a dimer. It accounts for possible two-MD defects along the chain, and for the disorder in the $(\times 2)$ direction which also affects the coherent domain width along the $(\times n)$ axis. Indeed, our calculation assumes a one-dimensional disorder, and therefore a surface consisting of Bi strips of six or seven unit mesh width. Because of the kinks in the MD lines (MDLs), or MD defects implying more than one unit, the disorder along the $(\times n)$ direction cannot be totally de-correlated from the one along the $(\times 2)$ axis.

When reconstructed blocks are stacked with disorder, but according to a periodic lattice, the diffracted intensity can be written as the Fourier transform of the pair correlation function [21, 22]. In the case of the Bi/Si surface, the need for a periodic lattice requires definition of at least seven (2×1) objects: A as the cell without a Bi dimer, B as the cell with the first Bi dimer, ... and G as the cell with the sixth dimer. Assuming a Markov chain of rank 1, the intensity can be calculated after diagonalization of the probability matrix $\mathbf{P}(1)$, of component $P_{X|Y}(1)$ the probability to find object X after object Y. The stacking being made of sequences of type ABCDEFA ... or ABCDEFGA ..., the matrix involves a single parameter p, the probability for object G to follow object F, that is the concentration of (2×7) cells. The non-zero components of $\mathbf{P}(1)$ are written $P_{B|A}(1) = P_{C|B}(1) = P_{D|C}(1) = P_{E|D}(1) = P_{F|E}(1) = P_{A|G}(1) = 1$, $P_{G|F}(1) = p$ and $P_{A|F}(1) = 1 - p$. Unfortunately, a computational approach is needed for diagonalization. Moreover, aggregation effects are not considered at all in such a model. Assuming $p = 0.5$ and labelling by 6 (7) the 2×6 (2×7) cell, one cannot distinguish a surface with sequences of type ... 666777 ... from a surface with sequences of type ... 676767 ....

Another approach is needed, which allows us to consider as elementary objects the (2×6) and (2×7) cells. The scattering generated by sequences of objects of different types, with phase shift between two consecutive objects depending on their type, was investigated in a pioneering work by Hendricks and Teller (HT) [23]. Recently, a general matrix scheme, the phase-matrix method [15, 24] has been developed, to calculate analytically the intensity diffracted by a succession of objects, of variable lengths and different structure factors. By incorporating phase terms inside the matrix $\mathbf{P}(1)$, the diagonalization problem is substituted by a matrix inversion. In the particular case of only two objects A (2×6) and B (2×7), with fixed lengths l_A and l_B, one could consider the formalism of HT. However, the matricial calculation proposed by Croset and de Beauvais [15] allows us to derive simpler analytical

expressions, depending only on the pair probabilities $P_{X|Y}(1)$, even increasing the number of objects. Moreover, the method allows us to treat explicitly the problem of finite size effects.

6.2. Intensity diffracted by a distribution of reconstructed blocks

Considering a chain of N objects, labelling by n the nth object (position $\boldsymbol{r}_n$), the diffracted intensity, averaged on all possible sequences of objects is written

$$\langle I\rangle = \sum_{n=1}^{N-1}\sum_{n'=n+1}^{N}\langle \mathrm{e}^{\mathrm{i}q(r_n-r_{n'})}F_nF_{n'}^*\rangle + \sum_{n=1}^{N-1}\sum_{n'=n+1}^{N}\langle \mathrm{e}^{-\mathrm{i}q(r_n-r_{n'})}F_n^*F_{n'}\rangle + \sum_{n=1}^{N}\langle F_nF_n^*\rangle \tag{1}$$

where F_n is the structure factor of the nth object, q is the momentum transfer. The generic term of the sum can be written, using labels X (Y) for the possible object states, and introducing the probability $P_X(n)$ to find the nth object in state X, as well as the probability $P_{Y|X}(n'-n)$ to find the n'th object in state Y knowing that the nth object is in state X

$$\langle \mathrm{e}^{\mathrm{i}q(r_n-r_{n'})}F_nF_{n'}^*\rangle = \sum_X\sum_Y P_X(n)F_XP_{Y|X}(n'-n)F_Y^*\,\mathrm{e}^{\mathrm{i}q(r_n-r_{n'})}. \tag{2}$$

Using matrix notation, the generic term takes the form:

$$\mathrm{e}^{\mathrm{i}q(r_n-r_{n'})}\,{}^t\boldsymbol{V}\,\mathbf{P}(n'-n)\boldsymbol{W} \tag{3}$$

where $\boldsymbol{V}$ is the vector of component F_Y^* (${}^t\boldsymbol{V}$ is the transpose of $\boldsymbol{V}$), $\boldsymbol{W}$ is the vector of component $P_X(n)F_X$, $\mathbf{P}(n'-n)$ is the matrix of component $P_{Y|X}(n'-n)$.

Introducing the matrix $\mathbf{T}(n'-n)$ of component

$$T_{Y|X}(n'-n) = \mathrm{e}^{-\mathrm{i}q(r_{n'}-r_n)}P_{Y|X}(n'-n) \tag{4}$$

we write

$${}^t\boldsymbol{V}\,\mathbf{T}(n'-n)\boldsymbol{W}. \tag{5}$$

Denoting by l_n the length of object n ($l_n = l_X$ if the nth object is in state X), we use the recurrent relation, $(r_{n'}-r_n) = (r_{n'-1}-r_n) + l_{n'-1}$, to obtain:

$$\mathrm{e}^{-\mathrm{i}q(r_{n'}-r_n)}P_{Y|X}(n'-n) = \sum_Z \mathrm{e}^{-\mathrm{i}ql_z}P_{Y|Z}(1)\,\mathrm{e}^{-\mathrm{i}q(r_{n'-1}-r_n)}P_{Z|X}(n'-1-n). \tag{6}$$

This is written in matrix notation

$$\mathbf{T}(n'-n) = \mathbf{T}(1)\,\mathbf{T}(n'-n-1) = \mathbf{T}(1)^{n'-n} \tag{7}$$

Recognizing that the generic term in summation (1) is the term of a geometric series, one can perform the calculation of $\langle I\rangle$ without need of matrix diagonalization. An immediate result is that the maxima of the intensity are given by the q-values which correspond to the minima of the determinant of $(\mathbf{I}d - \mathbf{T}(1))$ (noted $(Id - T)$ in the following).

Thus, for one crystallite, the intensity takes the form:

$$\langle I\rangle = 2\,\mathrm{Re}\left(\sum_{n=1}^{N-1}\sum_{n'=n+1}^{N}{}^t\boldsymbol{V}\,\mathbf{T}(1)^{n'-n}\boldsymbol{W}\right) + N\sum_X P_X(n)F_XF_X^* \tag{8}$$

where

$$\sum_{n=1}^{N-1}\sum_{n'=n+1}^{N}{}^t\boldsymbol{V}\,\mathbf{T}(1)^{n'-n}\boldsymbol{W} = \sum_{n=1}^{N-1}(N-n)\,{}^t\boldsymbol{V}\,\mathbf{T}(1)^{n-1}\,\mathbf{T}(1)\boldsymbol{W}. \tag{9}$$

Croset and de Beauvais [15] have shown that, so as to account for the experimental Lorentzian shape of the diffraction peaks, the single crystal 'cut-off' function $(N-n)$ must be replaced

by the sample 'cut-off' function $[\overline{N}\,\mathrm{e}^{-2n/\overline{N}}]$, where $\overline{N}$ is the mean size of the crystallites constituting the sample. The final intensity is written

$$\langle I\rangle = 2\overline{N}\,\mathrm{e}^{-2/\overline{N}}\,\mathrm{Re}({}^{t}\boldsymbol{V}(\mathbf{I}\boldsymbol{d}-\mathrm{e}^{-2/\overline{N}}\mathbf{T}(1))^{-1}\,\mathbf{T}(1)W)+\overline{N}\sum_{X}P_{x}(n)F_{X}F_{X}^{*}. \tag{10}$$

The $P_X(n)$ probabilities are related to the components of the $\mathbf{P}(1)$ matrix, using

$$\boldsymbol{P}(n)=\mathbf{P}(1)\boldsymbol{P}(n-1)=\mathbf{P}(1)^{n-1}\boldsymbol{P}(1) \tag{11}$$

where $\boldsymbol{P}(n)$ is the vector of component $P_X(n)$.

One assumes that the $P_X(n)$-values are independent of n, and correspond to the average concentration C_X of objects in state X. One eigenvalue (λ_1) of $\mathbf{P}(1)$ is equal to 1, while all others have their modulus strictly inferior to 1. Denoting by $\boldsymbol{S}$ the vector associated with $\lambda_1=1$, we have

$$\boldsymbol{P}(n)=\boldsymbol{P}(1)=\boldsymbol{S}. \tag{12}$$

6.3. Derivation of the pair probabilities $P_{XY(1)}$ from experimental profiles

The use of the matrix $\mathbf{T}$, built from the probability matrix $\mathbf{P}(1)$ of rank 7 with objects of length $l=b$ (b as the Si lattice parameter), leads to $\det(Id-T)=1-p\,\mathrm{e}^{-\mathrm{i}q7b}-(1-p)\,\mathrm{e}^{-\mathrm{i}q6b}$, where p is the probability to find a 2×7 cell instead of the 2×6 cell. Minima must be found at $\pm m/n$ from the integer order peaks, with m integer and $n=6.45$. This leads to $p=0.45$, a value which corresponds to an average length for the unit cell equal to $\langle l\rangle = p7b+(1-p)6b=nb$. One can verify that the intensity of the first satellite ($m=1$) is significantly higher than that of second orders.

The matrix $\mathbf{T}$, built with the objects A (2×6) and B (2×7) of respective length $6b$ and $7b$, leads to the following results. Using labels 6 and 7 instead of A and B, and notations $r=P_{AA}(1)=P_{66}$ and $q=P_{BB}(1)=P_{77}$, the $\mathbf{T}$ matrix is written

$$\mathbf{T}(1)=\begin{pmatrix}P_{66}\,\mathrm{e}^{-\mathrm{i}ql_6} & P_{67}\,\mathrm{e}^{-\mathrm{i}ql_7}\\ P_{76}\,\mathrm{e}^{-\mathrm{i}ql_6} & P_{77}\,\mathrm{e}^{-\mathrm{i}ql_7}\end{pmatrix}=\begin{pmatrix}r\,\mathrm{e}^{-\mathrm{i}ql_6} & (1-q)\,\mathrm{e}^{-\mathrm{i}ql_7}\\ (1-r)\,\mathrm{e}^{-\mathrm{i}ql_6} & q\,\mathrm{e}^{-\mathrm{i}ql_7}\end{pmatrix}. \tag{13}$$

The $P_X(n)$ probabilities are given by the vector associated to the eigenvalue $\lambda=1$ of $\mathbf{P}(1)$:

$$\boldsymbol{S}=\frac{1}{(2-q-r)}\begin{pmatrix}1-q\\1-r\end{pmatrix}=\boldsymbol{P}(n)=\begin{pmatrix}C_6\\C_7\end{pmatrix}. \tag{14}$$

The intensity should be found at a momentum transfer value $q=2\pi k$ with $k=0.155$ (or $k=0.845$). The constraint of a minimum of $y=|\det(Id-T)|^2$ at this k value ($\partial y/\partial k=0$) leads to a second order polynomial relation between r and q. One can extract several (q, r) sets of values, listed below. The corresponding C_7 values, and an order parameter, β, defined as $\beta=2-q-r$, are given ($\beta=0$ and $\beta=2$ correspond to the well ordered cases 666777 and 676767, while $\beta=1$ corresponds to a total disorder).

$q=P_{77}$	$r=P_{66}$	$P_7(n)=C_7$	β	$q=P_{77}$	$r=P_{66}$	$P_7(n)=C_7$	β
0.0	0.18	0.450	1.8	0.6	0.66	0.459	0.7
0.1	0.27	0.447	1.6	0.7	0.74	0.464	0.6
0.2	0.34	0.452	1.5	0.8	0.83	0.459	0.4
0.3	0.43	0.449	1.3	0.9	0.89	0.524	
0.4	0.50	0.454	1.1	1.0	0.91		
0.5	0.58	0.456	0.9				

(15)

All other (q, r) pairs produce peaks displaced from the experimental k-position. The limiting cases are $(q, r) = (0, 0)$ with peaks at $k = \pm m/13$, and (1, 1) with peaks at $k = \pm m/6$ and $k = \pm m/7$. One verifies in (15) that the experimental periodicity provides couples (q, r) leading to the same concentration $C_B = C_7$ of objects B (2×7 cell), whose value is close to the one found with objects of length b. The occurrence of peaks at location $k = 2\pi/(C_6 l_6 + C_7 l_7)$ can be derived from $\det(Id - T)$, if using C_7 and β, and making some approximations: $\det(Id - T) = 1 + (1 - \beta)(e^{-iql} + e^{-iql/2}) - e^{-iql/2(-1+\beta)}\, e^{-iq\beta(C_6 l_6 + C_7 l_7)}$, with $l = l_6 + l_7$.

As a first approximation, assuming $F_A = F_B$, one easily obtains the intensity (10) as the product of $(F_A\, F_A^*)$ by a function, periodic in k with period 1. This function depends on the $P_{A|A}(1)$ and $P_{B|B}(1)$ values, but applies the same to all peaks at $k = m \pm p/n$ with p fixed ($n = 6.45$ and m, p integers). This confirms that the refinement process can be performed disregarding disorder as produced by the probability distribution, when considering the first order satellites alone (at $k = m \pm 1/n$). So as to extract a single (q, r)-set, one needs to perform the calculation (10) using the values in table (15), then compare it with experimental data. In the one-dimensional scheme, the two possible structure factors F_A and F_B are:

$$F_A = e^{2i\pi k\delta} \sum_{m=1}^{5} e^{2i\pi k(m-1)d} \qquad \text{and} \qquad F_B = e^{2i\pi k\delta'} \sum_{m=1}^{6} e^{2i\pi k(m-1)d'} \quad (16)$$

where δ (δ') is related to the position of the first dimer in the 2×6 (2×7) cell and d (d') is related to the separation distance between dimers in the 2×6 (2×7) cell. According to the structural analysis, the dimers are almost equally spaced, with an average distance of 4.09 (4.065) Å in the 2×6 (2×7) cell, and a first dimer at 1.42 (1.47) Å in the 2×6 (2×7) cell. This leads to $d = 1.065$, $d' = 1.059$, $\delta = 0.370$ and $\delta' = 0.383$.

The more relevant parameter was the respective full widths at half maximum (FWHMs) of the first and second order satellites. Indeed, the FWHM of the peak at $k = 0.845$ is little affected by the values (q, r) with respect to that of the peak at $k = 0.69$. For instance, with $(q, r) = (0.60, 0.66)$, the second order satellite is split into two peaks, close to $k = 1 - 2/6$ and $k = 1 - 2/7$. This effect results from the aggregation tendency, as provided by the pair probability values, 0.60 for the 2×7 cell to follow a 2×7 cell, and 0.66 concerning the 2×6 cells. The splitting effect is reduced when using low $\overline{N}$ values, but still present. The set $(q, r) = (P_{77}, P_{66}) = (0.3, 0.43)$ was the best choice to fit the data, though the profiles were obtained using perpendicular scan conditions, while $\langle I \rangle$ is calculated along the $(\times n)$ direction (see the restrictive conditions in the geometry of the resolution function). Figure 6 shows the scans of the first and second order satellites, related to the in-plane peak $(h, k) = (1, -1)$ from the domain $(n \times 2)$. The k-profiles extracted from the calculation (10), with $\overline{N} = 5$, using the (q, r)-sets equal to (0.30, 0.43) and (0.60, 0.66), respectively, are drawn for comparison. The FWHM was multiplied in each case by a factor of four.

Using a distribution of (2×6) and (2×7) cells leads to a very small average number $\overline{N}$. As mentioned in section 6.1, relating the 1D model to the 2D Bi/Si surface, the $\overline{N}$-value should be associated with the frequency of kinks along the missing-dimer line, as well as the occurrence of defects like the two-missing-dimer one, or possible 2×5, 2×8 arrangements. In this context, as shown by the STM images of the 2×7 surface, ideally reconstructed domains do not extend more than six (2×7) units. Thus, the model was improved by incorporating a third object C, as the (2×1) cell without a Bi dimer, of length $l_1 = b$. Using the same notations as before (6 instead of A, 7 instead of B and 1 instead of C), we define a new probability $s = P_{16} = P_{17}$ and we assume $P_{61} = P_{71} = 1/2$, as well as $P_{11} = 0$.

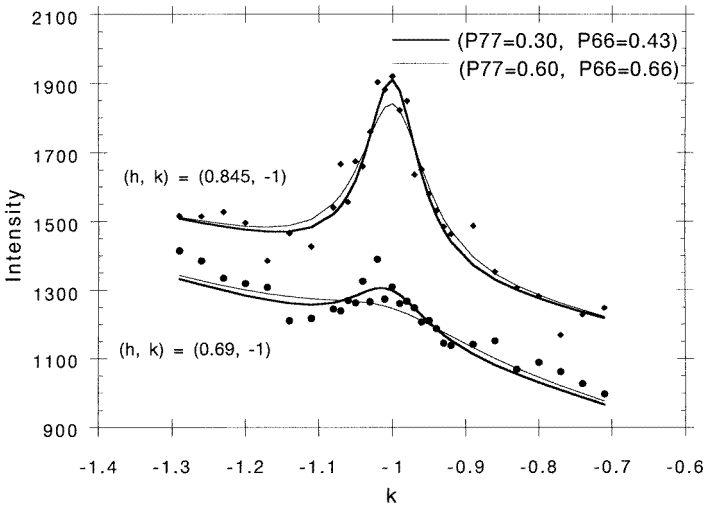

Figure 6. Experimental scans of reflections $(h, k) = (0.845, -1)$ and $(h, k) = (0.69, -1)$ from domain $(n \times 2)$, and associated profiles issuing from the calculation using $N = 5$ and $(q, r) = (P_{77}, P_{66}) = (0.30, 0.43)$ and (0.60, 0.66).

The $\mathbf{T}(1)$ matrix is written

$$\begin{pmatrix} r\,\mathrm{e}^{-\mathrm{i}ql_6} & (1-q-s)\,\mathrm{e}^{-\mathrm{i}ql_7} & \frac{1}{2}\,\mathrm{e}^{-\mathrm{i}ql_1} \\ (1-r-s)\,\mathrm{e}^{-\mathrm{i}ql_6} & q\,\mathrm{e}^{-\mathrm{i}ql_7} & \frac{1}{2}\,\mathrm{e}^{-\mathrm{i}ql_1} \\ s\,\mathrm{e}^{-\mathrm{i}ql_6} & s\,\mathrm{e}^{-\mathrm{i}ql_7} & 0 \end{pmatrix}. \tag{17}$$

The corresponding $P_X(n) = C_x$ values are given by

$$\boldsymbol{S} = \frac{1}{4-2q-2r-2s+2(r-q)s} \begin{pmatrix} 2-2q-s \\ 2-2r-s \\ 2(r-q)s \end{pmatrix} = \boldsymbol{P}(n) = \begin{pmatrix} C_6 \\ C_7 \\ C_1 \end{pmatrix}. \tag{18}$$

The constraint of a minimum of $y = |\det(Id - T)|^2$ at $k = 0.155$ allows us to derive different (q, r)-sets fixing the s-value. One can observe that for $s > 0.3$, the peaks are split, one component arising near $k = 1/8$, owing to the occurrence in the chain of (2×8) cells, with six Bi dimers and two missing dimers. Provided that s is kept lower than 0.3, one observes a significant enlargement in the width of the peaks, as well as a decrease in the intensity ratio I_1/I_2 of the first and second order satellites, compared with the two-object case. Using large $\overline{N}$-values, the experimental ratio I_1/I_2 is retrieved at $s = 0.3$ for (q, r) between (0.4, 0.674) and (0.6, 0.676). These values give concentrations (C_6, C_7, C_1) equal to (0.63, 0.25, 0.12) and (0.56, 0.39, 0.05) respectively. However, some splitting is found on the second order satellites. For these peaks, owing to the low resolution in k as produced by the scanning requirements, we cannot proceed to the refinement on the $(\overline{N}, q, r, s)$-set confidently. Retaining the (q, r)-values found with $s = 0.3$ (large $\overline{N}$), we verify that the concentration of two missing dimers is weak, that of (2×6) cells being slightly changed compared with the value found in the two-object model. The concentration C_7 is reduced, as a logical consequence of possible (2×6)-(2×1) arrangements. The pair probabilities $P_{X|X}(1)$ are found to be larger, but still reflect a weak tendency to aggregation.

7. Conclusion

With the Bi/Si(001)-$(2 \times n)$ interface ($n = 6.45$), we give evidence that the GIXD technique allows the structural determination of surfaces with restricted long-range order. The integrated intensities must be corrected by the active area of the reciprocal lattice node, given by the trace of the resolution function during scanning. In spite of the loss in accuracy on the atomic positions, we provide the first estimation of the lateral spacing between the $(n - 1)$ Bi dimers inside a $(2 \times n)$ block ($= 6, 7$). They are equally spaced by 4.1 Å, in comparison with 3.84 Å for Si atoms. Thus, the misfit stress between Bi and Si is relieved both by the missing-dimer (MD) defect, and the displacements of the dimers inside the block towards this MD. This feature has been neglected in all previous reports on the bonding geometry of the Bi/Si interface. The Bi dimer bond length is found to be equal to 3.11 ± 0.01 Å, while the underlying Si atoms are at bulk positions (except those near the vacancy). This confirms the breaking of the Si dimers with Bi adsorption. The height of the Bi layer with respect to Si is 1.88 ± 0.02 Å.

We reproduce the intensity profiles corresponding to the $n = 6.45$ periodicity, by use of the phase-matrix method. When (2×6) and (2×7) cells are considered exclusively, we derive a probability value for the (2×6) cell to follow a (2×6) cell equal to 0.4, while this value is equal to 0.3 concerning the (2×7) cells. This tendency to stacking disorder should result from similar values of the (2×6) and (2×7) minimum-energy configurations. As a matter of fact, we found the dimer block incommensurate with respect to Si. Thus, a deviation of one dimer length in the dimer blocks is not expected to affect the interaction between the missing dimers along the $(\times n)$-axis.

The final sequence of missing-dimer lines with more or fewer kinks is the result of a strength balance of two types of interaction between vacancies: the long-range repulsive one between missing-dimer lines (along $(\times n)$) and the short-range attractive one between missing dimers (along $(\times 2)$). The small value found for the number $\overline{N}$ of correlated objects, along a chain of (2×6) and (2×7) blocks, demonstrates that the long-range interaction is not de-correlated from the short-range one between missing dimers. As a matter of fact, one can use high $\overline{N}$-values when considering the possibility of two missing dimers. In the case of a striped array of domains with repulsive interaction between domain boundaries, a relation was proposed between the size of a single domain and the minimum separation between them [25]. This relation seems not valid on the Bi/Si interface, for which the one-missing-dimer defect is mainly implicated, in contrast to the clean $(2 \times n)$ Si surface, where the defects are two missing dimers [11]. Theoretical extension, on the basis of the elastic constants that could be deduced from our model, as well as on the basis of the probability distribution, would be of great interest.

Acknowledgments

The authors express their thanks to K Aid, M Sauvage-Simkin and R Pinchaux for helpful discussions and support during experiments.

References

[1] Hanada T and Kawai M 1991 *Surf. Sci.* **242** 137
[2] Park Ch, Bakhtizin R Z, Hashizume T and Sakurai T 1993 *Japan. J. Appl. Phys.* **32** L528
[3] Michailov M and Gutzow I (eds) 1994 *Proc. East–West Surface Science Workshop on Thin Films and Phase Transitions on Surfaces (Bulgarian Academy of Science, Sofia, 1994)*
[4] Nagl C, Pinczolits M, Schmid M, Varga P and Robinson I K 1995 *Phys. Rev.* B **52** 16 796
[5] Sakamoto K, Kyoya K, Miki K and Matsuhata H 1993 *Japan. J. Appl. Phys.* **32** L204

[6] Noh H P, Park Ch, Jeon D, Cho K, Hashizume T, Kuk Y and Sakurai T 1994 *J. Vac. Sci. Technol.* B **12** 2097
[7] Aruga T and Murata Y 1986 *Phys. Rev.* B **34** 5654
[8] Martin J A, Savage D E, Moritz W and Lagally M G 1986 *Phys. Rev. Lett.* **56** 1936
[9] Louwsma H K, Zandvliet H J W, Kersten B A G, Chesneau J, van Silfhout A and Poelsema B 1997 *Surf. Sci.* **381** L594
[10] Richter M *et al* 1990 *Phys. Rev. Lett.* **65** 3417
[11] Zandvliet H J W, Louwsma H K, Hegeman P E and Poelsema B 1995 *Phys. Rev. Lett.* **75** 3890
[12] Safran S A 1980 *Phys. Rev. Lett.* **44** 937
Millman S E and Kirczenow G 1982 *Phys. Rev.* B **26** 2310
[13] Nishitani R, Uno Y and Suematsu H 1983 *Phys. Rev.* B **27** 6572
[14] Park Ch, Bakhtizin R Z, Hashizume T and Sakurai T 1994 *J. Vac. Sci. Technol.* B **12** 2049
[15] Croset B and de Beauvais C 1998 *Surf. Sci.* **409** 403
[16] Jedrecy N, Sauvage-Simkin M, Pinchaux R, Masies J, Greiser N and Etgens V H 1990 *Surf. Sci.* **230** 197
Felici R, Robinson I K, Ottaviani C, Imperatori P, Eng P and Perfetti P 1997 *Surf. Sci.* **375** 55
[17] Vlieg E 1997 *J. Appl. Cryst.* **30** 532
[18] The residual χ^2 is defined as $\chi^2 = (N-p)^{-1}\sum(F_{obs} - |F_{calc}|)^2/\sigma^2$, where σ is the error bar on F_{obs}, N the number of reflections and p the number of fitting parameters. One can also consider the reliability factor R defined by $R = \sum(F_{obs} - |F_{calc}|)^2 / \sum(F_{obs})^2$.
[19] Tang S and Freeman A J 1994 *Phys. Rev.* B **50** 1701
[20] Franklin G E, Tang S, Woicik J C, Bedzyk M J, Freeman A J and Golovchenko J A 1995 *Phys. Rev.* B **52** R5515
[21] Garreau Y, Sauvage-Simkin M, Jedrecy N, Pinchaux R and Veron M B 1996 *Phys. Rev.* B **54** 17 638
[22] Lent C S and Cohen P I 1984 *Surf. Sci.* **139** 121
[23] Hendricks S and Teller E 1942 *J. Chem. Phys.* **10** 147
[24] Uimin G and Lindgard P-A 1997 *Acta Crystallogr.* A **53** 15
[25] Zeppenfeld P, Krzyzowski M, Romainczyk C, Comsa G and Lagally M G 1994 *Phys. Rev. Lett.* **72** 2737